SIAM J. APPL. MATH.
Vol. 58, No. 3, pp. 961–974, June 1998
© 1998 Society for Industrial and Applied Mathematics
013

Downloaded 03/31/14 to 128.210.126.199. Redistribution subject to SIAM license or copyright; see http://www.siam.org/journals/ojsa.php

A PARALLEL SHOOTING METHOD FOR DETERMINING THE NATURAL SHAPE OF A LARGE SCIENTIFIC BALLOON*

FRANK BAGINSKI†, WILLIAM COLLIER†, AND TAMI WILLIAMS†

Abstract. Large scientific balloons provide a dependable low cost platform for carrying out research in the upper atmosphere. Usually, the design of such a balloon is based on an axisymmetric natural shape defined by the solutions of a mathematical model derived by researchers at the University of Minnesota in the 1950s. For a natural-shape balloon, all the tension in the balloon fabric is carried in the meridional direction and the circumferential stress is assumed to be zero. In this paper, we will establish existence results for the model equations and present numerical solutions for a variety of parameters. For the case of a balloon at float altitude, the model equations can be solved by an ordinary shooting method. To model axisymmetric ascent shapes, one needs to make some crude assumptions on how excess film is handled. When the volume of the lifting gas is very small, the ordinary shooting method is ineffective for computing axisymmetric ascent shapes. In the past, ad hoc assumptions were employed to circumvent this difficulty. In the work presented here, a parallel shooting method is used to determine these shapes without the need of additional assumptions.

Key words. balloon shapes, axisymmetric membranes, parallel shooting method

AMS subject classifications. 34B15, 65L10, 73K10

PII. S0036139995292355

1. Introduction.

Large scientific balloons provide a dependable low cost platform for carrying out research in the upper atmosphere. To maintain a payload at a fixed altitude, Archimedes' principle states that the balloon must displace an amount of air whose weight is equal to the balloon system (payload, film weight, load tapes, ballast, gondola, etc.). In the upper atmosphere the air is very thin, so that the volume of the balloon at its float altitude is extremely large. For example, to carry a 5,000 lb payload to an altitude of 126,000 feet, a balloon whose total volume at float is approximately 39.96 million cubic feet is needed. The balloon itself weighs about 2000 lbs with a total surface area of about 20 acres. The balloon is constructed from long, thin tapered sheets of polyethylene called gores that are sealed edge to edge to form a complete shape. For a 39.96 mcf. balloon, about 170 gores are needed for a complete shape. Each gore is about 600 feet in length with a maximum width of about 8 feet.

In a simplified balloon system consisting of the balloon envelope and payload, Archimedes' principle leads to the following condition at the float altitude,

$$w_d \mathcal{A}_d + L = b_d \mathcal{V}_d, \tag{1.1}$$

where $\mathcal{V}_d$ is the volume of the lifting gas, b_d is the specific buoyancy, w_d is the film weight per unit area, and $\mathcal{A}_d$ is the surface area of the balloon. In the following, a subscript "d" indicates that the associated quantity applies to the design or float shape. Below the design altitude, a similar equation must hold,

$$W_{film} + L = b\mathcal{V}, \tag{1.2}$$

*Received by the editors September 25, 1995; accepted for publication August 25, 1997; published electronically April 29, 1998. This research was supported by NASA grant NAG5-697.
http://www.siam.org/journals/siap/58-3/29235.html
†Department of Mathematics, George Washington University, Washington, DC 20052 (frank@math.gwu.edu, collier@math.gwu.edu, tami@athena.math.gwu.edu).

Downloaded 03/31/14 to 128.210.126.199. Redistribution subject to SIAM license or copyright; see http://www.siam.org/journals/ojsa.php

where $W_{film} = w_d \mathcal{A}_d$, $\mathcal{V} < \mathcal{V}_d$ is the volume of the gas bubble, and $b > b_d$ is the appropriate buoyancy constant for that altitude. Typically a balloon is designed to carry a given payload to a fixed altitude, so that L, b_d, and w_d are known. One of the first steps in the design process is to determine the shape of the balloon at float, i.e., the design shape. A real balloon at float will assume a cyclic shape (depending on the number of gores used in its construction), rather than a pure axisymmetric shape. However, for design purposes, an axisymmetric shape model gives a good first approximation. We will consider also the problem of determining axisymmetric ascent shapes (i.e., shapes below the design altitude). We will not consider the dynamics of a balloon at launch or its flight to float altitude. Our shapes are quasi-steady state in the sense that they are computed for a fixed altitude.

Design of the float shape is based usually on an axisymmetric model that was developed by researchers at the University of Minnesota [1] in the 1950s. In this model, a system of nonlinear differential equations in the form $\mathbf{y}' = \mathbf{h}(\mathbf{y})$ with appropriate boundary conditions must be solved. The model equations are often referred to as the Σ-shape equations, named so for a key parameter Σ that appears in the rescaled equations. These equations were solved initially using an analogue computer for a variety of conditions (see [1]). In a series of reports based on this model (see, e.g., [9]), Justin Smalley carried out extensive numerical computations using a digital computer. In this work, we will be concerned with *natural-shape* balloons, i.e., shapes in which the balloon fabric is assumed to have zero circumferential stress and all tension is carried in the meridional direction.

Smalley went on to consider shapes below the design altitude (see [10]). While ascending to float, the balloon envelope is not fully deployed. The volume of the lifting gas is less than the corresponding volume at float, and excess balloon fabric needs to be accounted for. To keep the simplicity of the axisymmetric model, Smalley made the assumption that the excess material was distributed symmetrically (this means that the "effective" film weight per unit area is increased so that (1.2) is satisfied for $\mathcal{V} < \mathcal{V}_d$). Based on our numerical results, an ordinary shooting method can be employed to solve the governing equations as long as $\mathcal{V}$ is larger than 10% of $\mathcal{V}_d$. For smaller volumes, this procedure is not effective. Let $(z(s), r(s))$ denote the generating curve for the axisymmetric balloon shape (ascent or float) where $0 \le s \le \ell_d$ and ℓ_d denotes the length of a meridian. Because balloons are constructed from long tapered sheets of polyethylene called gores, the quantity ℓ_d is referred to as the gore length (see [8, Sec. 5]). Let $\theta(s)$ be the angle that the tangent makes with the z-axis (see Figure 2.1). When $\mathcal{V} \le 0.10 \cdot \mathcal{V}_d$, then $\theta(0) \approx 0.0^\circ$ and it becomes exceedingly difficult to satisfy the boundary conditions for a natural-shape balloon. Smalley circumvented this difficulty by assuming that $(z(s), r(s)) = (s, 0)$ for $0 \le s \le s^*$. The value of s^* was chosen in an ad hoc way with $\theta(s^*) \approx 0.5^\circ$ (see [10, p. 2]). Excess fabric (i.e., fabric that is not needed to form the boundary of the gas bubble) is assumed to hang in a rope section at the base of the balloon. The weight of this material corresponding to $0 \le s \le s^*$ was added to the payload. Alternatively, one could assume that the weight per unit area of the balloon remains fixed and all excess film weight is added to the payload (see [3]). Real ascent shapes are clearly nonaxisymmetic and have a very complicated geometry that includes internally folded material, a periodic lobe pattern surrounding the gas bubble, and flat wing-like structures below the gas bubble. These types of shapes will not be discussed here (see [4], [5] for further details on modeling nonaxisymmetric shapes). Even though the axisymmetric ascent model might not provide valid data such as the stress in the film, it does provide information such as

Downloaded 03/31/14 to 128.210.126.199. Redistribution subject to SIAM license or copyright; see http://www.siam.org/journals/ojsa.php

the pressure and gas volume that may be of practical use. The utility of the Σ-shape equations as a model for the float shape is demonstrated by the numerous successful missions supported by large scientific balloons that are based on the Σ-shape design.

In the work presented here, we provide a mathematical setting in which existence results for the model equations can be established. These results follow from the standard theory of nonlinear boundary value problems, since $\partial \mathbf{h}/\partial \mathbf{y}$ is continuous. Because of the way the balloon problem is formulated, we should not expect uniqueness. This was first suggested by the double-cell configuration presented in [1, Vol. I, p. 3–14] (double- and triple-cell configurations are presented in section 4.1). For ℓ_d sufficiently large, numerical calculations suggest that a balloon shape with k cells for any number k is possible. The multicell configurations are not of practical use, since they would be very difficult to handle during the launch phase. Moreover, since a single cell shape will require less surface area than a multicell shape enclosing the same volume, the single cell shape is the more efficient of the two.

It is important to consider shapes in the range $\mathcal{V} < 0.1 \cdot \mathcal{V}_d$, because at launch the volume of the gas bubble is less than 1% of its float volume. We found that by applying a parallel shooting method, we were able to compute solutions for very small gas bubbles without the need of the ad hoc assumption made by Smalley. Our results using a parallel shooting method are in agreement with those presented by Smalley (see Tables 4.1, 4.2 of section 4.2 and [10, Tables 1 and 3], respectively).

Although the equilibrium equations for an axisymmetric balloon are well known (see, e.g., [1], [8], [9], [10]), we include a brief derivation for the convenience of the reader, because previous treatments are given in technical reports that are not readily available. Following the approach of Antman (see [2]), we obtain the standard Σ-shape model equations in section 2. In section 3, we introduce the equations for a natural-shape balloon with appropriate boundary conditions for float and ascent. In section 4.1, we present a number of numerical results, including float shapes with zero film weight for single-, double-, and triple-cell configurations. A design shape and a family of axisymmetric ascent shapes with nonzero film weight is presented in section 4.2.

2. Equilibrium equations for a natural-shaped balloon. The equations for an axisymmetric balloon shape were first derived by researchers at the University of Minnesota (see [1]). A derivation of these equations is presented in [8, Sec. V]. Numerical solutions were obtained via analogue computer (see [1]). More extensive computations were carried out on a digital computer by Smalley (see, e.g., [9], [10]). Because these treatments appear in technical reports that are not readily available, we include a brief derivation of the equilibrium equations for an axisymmetric balloon shape in this section. We follow the approach presented by Antman (see [2, pp. 343–346]) and model the balloon as an axisymmetric membrane. We begin with some notation and then give some physical justification for the governing equations. While the treatment follows the approach of [2], we use the standard notation contained in most technical reports on ballooning (see [8]). We differ from Antman's convention in that the equilibrium equations are expressed relative to the deformed configuration, which is consistent with the derivation in [8].

Since we seek axisymmetric solutions, we need to find a generating curve $s \to (z(s), r(s))$, where s is the arc-length. Let ℓ_d be the total length of the generating curve. We can express the solution as $\mathbf{x}(s, \phi)$ (see Figure 2.1), where $s \in [0, \ell_d]$, $\phi \in [0, 2\pi]$, and

Downloaded 03/31/14 to 128.210.126.199. Redistribution subject to SIAM license or copyright; see http://www.siam.org/journals/ojsa.php

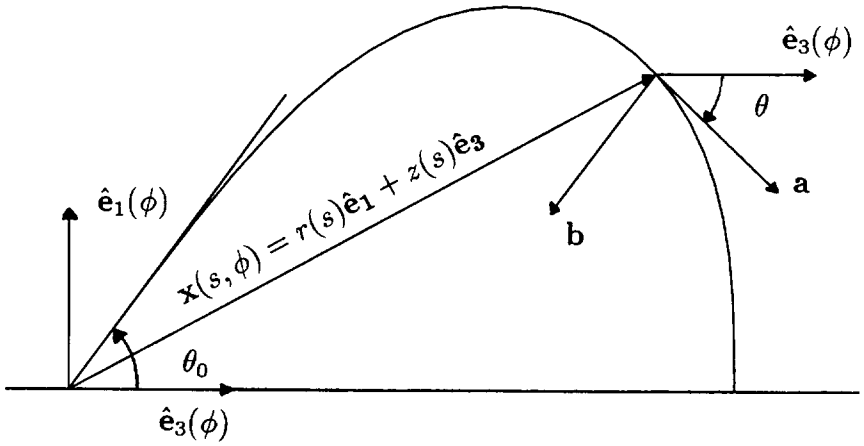

FIG. 2.1. *Generating curve for a natural-shape balloon (at float).*

$$\begin{aligned}\mathbf{x}(s,\phi) &= r(s)\hat{\mathbf{e}}_1(\phi) + z(s)\hat{\mathbf{e}}_3(\phi),\\ \hat{\mathbf{e}}_1(\phi) &= \cos\phi\mathbf{i} + \sin\phi\mathbf{j},\\ \hat{\mathbf{e}}_3(\phi) &= \mathbf{k}.\end{aligned}$$

It is also useful to define $\hat{\mathbf{e}}_2(\phi)$ to be the unit vector which completes the right-hand triad $\{\hat{\mathbf{e}}_1, \hat{\mathbf{e}}_2, \hat{\mathbf{e}}_3\}$,

$$\hat{\mathbf{e}}_2(\phi) = \hat{\mathbf{e}}_3(\phi) \times \hat{\mathbf{e}}_1(\phi) = -\sin\phi\mathbf{i} + \cos\phi\mathbf{j}. \tag{2.1}$$

The balloon's shape is defined by the parametrized surface,

$$\mathcal{S} = \{\mathbf{x}(s,\phi) \mid s \in [0,\ell_d], \phi \in [0,2\pi]\}. \tag{2.2}$$

At each point along the curve, $s \to \mathbf{x}(s,\phi)$, the tangent vector is given by

$$\mathbf{a}(s,\phi) = \frac{\partial \mathbf{x}}{\partial s}(s,\phi) = \sin\theta(s)\hat{\mathbf{e}}_1(\phi) + \cos\theta(s)\hat{\mathbf{e}}_3(\phi), \tag{2.3}$$

where $\theta(s)$ is the angle between $\mathbf{a}$ and $\hat{\mathbf{e}}_3(\phi)$ (see Figure 2.1), $z'(s) = \cos\theta(s)$, and $r'(s) = \sin\theta(s)$. The inward pointing normal is

$$\mathbf{b}(s,\phi) = \mathbf{a} \times \hat{\mathbf{e}}_2(\phi) = -\cos\theta\hat{\mathbf{e}}_1(\phi) + \sin\theta\hat{\mathbf{e}}_3(\phi). \tag{2.4}$$

Let $s_0 \in [0,\ell_d]$, and let the vector $\mathbf{n}_1(s_0,\phi)$ denote the resultant stress defined at each point of the curve $\phi \to \mathbf{x}(s_0,\phi)$. Then $\mathbf{n}_1(s_0,\phi)$ represents the density of the resultant contact force generated by the part of $\mathcal{S}$ with $s \geq s_0$ acting on the portion of $\mathcal{S}$ with $s < s_0$. Similarly, let $0 \leq \phi_0 < 2\pi$ and let $\mathbf{n}_2(s,\phi_0)$ denote the resultant stress defined at each point of the curve $s \to \mathbf{x}(s,\phi_0)$. The vector $\mathbf{n}_2(s,\phi_0)$ represents the density of resultant contact force generated by the part of $\mathcal{S}$ with $\phi_0 \leq \phi < \phi_0 + \epsilon$ acting on the part of $\mathcal{S}$ with $\phi_0 - \epsilon < \phi < \phi_0$. We choose $\epsilon > 0$ small enough that $0 \leq \phi_0 - \epsilon$ and $\phi_0 + \epsilon \leq 2\pi$. Both $\mathbf{n}_1$ and $\mathbf{n}_2$ are measured per unit length in the deformed configuration.

Because the balloon is modeled as a membrane, we can ignore all bending moments and couples. Furthermore, under the assumption of axisymmetry, we can write

Downloaded 03/31/14 to 128.210.126.199. Redistribution subject to SIAM license or copyright; see http://www.siam.org/journals/ojsa.php

the contact forces as

$$\mathbf{n}_1(s,\phi) = \sigma_m(s)\mathbf{a}(s,\phi),$$
$$\mathbf{n}_2(s,\phi) = \sigma_c(s)\hat{\mathbf{e}}_2(\phi),$$

where σ_m is the meridional stress and σ_c the circumferential stress.

Next, we investigate the equilibrium of a test patch $\mathcal{A}$, where

$$\mathcal{A} = \{\mathbf{x}(\xi,\psi) \mid s_0 \le \xi \le s,\ 0 \le \psi \le \phi\}$$

for some $s_0 \in (0,\ell_d)$ and $\phi \in (0,2\pi)$. The forces acting on $\mathcal{A}$ are the internal forces, $\mathbf{n}_1(s,\phi)$ and $\mathbf{n}_2(s,\phi)$, and the external forces,

$$\mathbf{f}(s,\phi) = -p(s)\mathbf{b}(s,\phi) - w(s)\hat{\mathbf{e}}_3(\phi),$$

where p is hydrostatic pressure due to the difference between the densities of the lifting gas and the ambient air and w is balloon film weight per unit area of the deformed configuration. We allow w to depend on s when computing axisymmetric ascent shapes, although when computing the float shape, w is generally assumed to be constant. The total force acting on $\mathcal{A}$ is

$$0 = \int_0^\phi \sigma_m(s)\mathbf{a}(s,\psi)r(s)d\psi - \int_0^\phi \sigma_m(s_0)\mathbf{a}(s_0,\psi)r(s_0)d\psi + \int_{s_0}^s \sigma_c(\xi)\hat{\mathbf{e}}_2(\phi)d\xi - \int_{s_0}^s \sigma_c(\xi)\hat{\mathbf{e}}_2(0)d\xi + \int_{s_0}^s \int_0^\phi \mathbf{f}(\xi,\psi)r(\xi)d\psi d\xi. \tag{2.5}$$

Differentiating (2.5) with respect to s and ϕ and using $\partial\hat{\mathbf{e}}_2/\partial\phi = -\hat{\mathbf{e}}_1$, we are led to the following equilibrium equations:

$$\frac{\partial}{\partial s}(r\sigma_m\mathbf{a}) - \sigma_c\hat{\mathbf{e}}_1(\phi) + r\mathbf{f} = \mathbf{0}. \tag{2.6}$$

3. The Σ-shape model equations. In this section, we formulate the Σ-shape model, including boundary conditions for the float and ascent shapes. Projecting (2.6) onto the $\hat{\mathbf{e}}_3(\phi)$ and $\hat{\mathbf{e}}_1(\phi)$ directions, we obtain

$$0 = \frac{d}{ds}(r\sigma_m\cos\theta) - rw - pr\sin\theta, \tag{3.1}$$

$$0 = \frac{d}{ds}(r\sigma_m\sin\theta) - \sigma_c + pr\cos\theta, \tag{3.2}$$

respectively. When considering shapes below float, we will allow $w(s)$ to vary as a function of s in order to satisfy an equilibrium condition. After carrying out the differentiation and rearranging terms in (3.1)–(3.2), we obtain

$$0 = \frac{d}{ds}(r\sigma_m)\cos\theta - (r\sigma_m)\sin\theta\frac{d\theta}{ds} - rw - pr\sin\theta, \tag{3.3}$$

$$0 = \frac{d}{ds}(r\sigma_m)\sin\theta + (r\sigma_m)\cos\theta\frac{d\theta}{ds} - \sigma_c + pr\cos\theta. \tag{3.4}$$

If we substitute $p = b(z+a)$, where a is the distance from the zero-pressure level to the bottom of the balloon and b is the specific buoyancy of the lifting gas, and solve

Downloaded 03/31/14 to 128.210.126.199. Redistribution subject to SIAM license or copyright; see http://www.siam.org/journals/ojsa.php

for $d\theta/ds$ and $d(r\sigma_m)/ds$, we obtain

$$(r\sigma_m)\frac{d\theta}{ds} = \sigma_c \cos\theta - rw\sin\theta - br(z+a), \tag{3.5}$$

$$\frac{d}{ds}(r\sigma_m) = \sigma_c \sin\theta + rw\cos\theta. \tag{3.6}$$

While b is known as a function of altitude, a is determined by boundary conditions and certain parameters. A solution is computed for a fixed altitude, so there are no kinetic terms present.

Since the generating curve is parametrized by arc-length, we see that

$$\frac{dz}{ds} = \cos\theta, \qquad \frac{dr}{ds} = \sin\theta. \tag{3.7}$$

Letting $A(s)$ denote the area of the surface of revolution between $z = z(0)$ and $z = z(s)$, we see that

$$\frac{dA}{ds} = 2\pi r. \tag{3.8}$$

Similarly, if $V(s)$ is the volume of the surface of revolution, we see that

$$\frac{dV}{ds} = \pi r^2 \frac{dz}{ds} = \pi r^2 \cos\theta. \tag{3.9}$$

The total film load T in the meridional direction is defined to be

$$T = 2\pi(r\sigma_m). \tag{3.10}$$

For applications considered here, we will assume that a load L is suspended from the base of the balloon. Thus,

$$T(0) = \frac{L}{\cos\theta_0}, \tag{3.11}$$

where $\theta(0) = \theta_0$ and θ_0 is one-half the "cone-angle" at the base of the balloon (see Figure 2.1). Note that θ_0 is not known a priori and must be computed based on certain parameter values and boundary conditions. If there is no load at the top of the balloon, then $\theta = -\pi/2$ at the top. Under the assumption of a natural shape, all the tension is in the meridional direction, so that $\sigma_c = 0$.

It is convenient to rescale the model equations. Following the notation of [8], we let

$$\lambda = \left(\frac{L}{b_d}\right)^{1/3}, \tag{3.12}$$

where b_d is the specific buoyancy at float. For certain balloon systems, various instruments, valves, or control devices are positioned on a small platform located at the top of the balloon. In general, the payload need not be located at the base of the balloon. In this case, we would define $\lambda = (P/b_d)^{1/3}$, where P is the total payload. We will not consider such configurations in our work presented here. See [8] for further discussion of these types of systems.

For our applications, the gross weight G is the sum of the total film weight W_{film} plus the load L. At float altitude, the balloon is fully deployed, the zero-pressure level

Downloaded 03/31/14 to 128.210.126.199. Redistribution subject to SIAM license or copyright; see http://www.siam.org/journals/ojsa.php

is at the base of the balloon (i.e., $a = 0$), w_d is known, and (1.1) is satisfied naturally by a solution of (3.1)–(3.2). To see this, we first set $p = b(z + a)$ and $\sin\theta = dr/ds$ in (3.1) and obtain

$$\frac{d}{ds}(r\sigma_m \cos\theta) = rw + b(z + a)\frac{dr}{ds}. \tag{3.13}$$

If we let ℓ_d denote the length of a meridian and integrate (3.13) from 0 to ℓ_d, we obtain

$$(r\sigma_m)(\ell_d)\cos\theta(\ell_d) - (r\sigma_m)(0)\cos\theta(0) = \int_0^{\ell_d} w(s)r(s)ds + b\int_0^{\ell_d}(z(s) + a)r(s)\frac{dr}{ds}ds. \tag{3.14}$$

Since

$$r\frac{dr}{ds}(z + a) = \frac{1}{2}\frac{d}{ds}[r^2(z + a)] - \frac{1}{2}r^2\frac{dz}{ds},$$

we see that (3.14) can be written in the form

$$(r\sigma_m)(\ell_d)\cos\theta(\ell_d) - (r\sigma_m)(0)\cos\theta(0) = \int_0^{\ell_d} w(s)r(s)ds + \frac{b}{2}\int_0^{\ell_d}\left(\frac{d}{ds}[r^2(z + a)] - r^2\frac{dz}{ds}\right)ds. \tag{3.15}$$

At float, $b = b_d$ and $a = 0$. Using the boundary conditions, $r(0) = r(\ell_d) = 0$ and $\theta(\ell_d) = -\frac{1}{2}\pi$, and multiplying (3.15) by 2π, we find

$$-2\pi(r\sigma_m)(0)\cos\theta_0 = \int_0^{\ell_d} 2\pi w(s)r(s)ds - b_d\int_0^{z(\ell_d)} \pi r^2(z)dz. \tag{3.16}$$

Applying (3.10)–(3.11) to (3.16), we obtain

$$-L = W_{film} - b_d\mathcal{V}_d, \tag{3.17}$$

which after rearrangement is (1.1). Note that θ_0, ℓ_d, and $z(\ell_d)$ are unknowns and are computed based on the design criteria of the balloon.

Let $\mathcal{V}$ denote the volume of the balloon for some fixed altitude during ascent. Let $\mathcal{A}$ denote the surface area of the corresponding shape. At such an altitude, $a < 0$, $\mathcal{V} < \mathcal{V}_d$, and $\mathcal{A} < \mathcal{A}_d$. To preserve the total weight of the balloon film, we will assume that the film weight $w(s)$ is in the form

$$w(s) = w_d\rho(s). \tag{3.18}$$

At float, $\rho(s) = 1$ and below the design altitude, we set $\rho(s) = R_d(s)/r(s)$, where

$$(Z_d(s), R_d(s)), \quad 0 \le s \le \ell_d, \tag{3.19}$$

is the generating curve for the float shape and $(z(s), r(s))$ is the corresponding curve for an ascent shape (while it appears there may be some difficulties with this definition at $s = 0$ and $s = \ell_d$, it will turn out that the relevant equations will be well defined

Downloaded 03/31/14 to 128.210.126.199. Redistribution subject to SIAM license or copyright; see http://www.siam.org/journals/ojsa.php

at the zeros of r). The total weight of the balloon with generating curve $(z(s), r(s))$ is W_{film}, since the length of a meridian for float and ascent shapes is ℓ_d, and

$$2\pi \int_0^{\ell_d} w(s)r(s)ds = 2\pi \int_0^{\ell_d} w_d R_d(s)ds = w_d \mathcal{A}_d = W_{film}. \tag{3.20}$$

Under these conditions, the gross weight $G = W_{film} + L$ for all altitudes.

Dividing (1.1) by L, and using the definition of λ, we see that λ has the units of length (see [8, p. 8]). Before rescaling the equations, we introduce the parameter Σ as defined in [1], i.e.,

$$\Sigma = \left(\frac{2\pi}{L}\right)^{1/3} \left(\frac{V}{G}\right)^{2/3} w_d. \tag{3.21}$$

We will follow the convention in [8], where Σ is defined as

$$\Sigma = (2\pi)^{1/3} \frac{w_d}{b_d \lambda}. \tag{3.22}$$

It is a straightforward exercise to show that the definitions of Σ given in (3.21)–(3.22) are equivalent. Next, we introduce new parameters and variables,

$$\bar{a} = \frac{a}{\lambda}, \quad \bar{r} = \frac{r}{\lambda}, \quad \bar{z} = \frac{z}{\lambda}, \quad \bar{s} = \frac{s}{\lambda}, \quad k\,\Sigma = \frac{\Sigma}{(2\pi)^{1/3}} = \frac{w_d}{b_d \lambda}, \quad \bar{\sigma}_m = \frac{\sigma_m}{b_d \lambda^2}, \tag{3.23}$$

where $k = 1/\sqrt[3]{2\pi}$. The function ρ is invariant under the scaling by λ since $\bar{\rho} = \bar{R}_d/\bar{r} = (\lambda R_d)/(\lambda r) = R_d/r = \rho$. Since $d\bar{s}/ds = 1/\lambda$ and

$$\frac{d\theta}{ds} = \frac{d\theta}{d\bar{s}} \frac{d\bar{s}}{ds} = \frac{d\theta}{d\bar{s}} \frac{1}{\lambda},$$

we see

$$\frac{dr}{ds} = \frac{dr}{d\bar{s}} \frac{1}{\lambda} = \frac{d\bar{r}}{d\bar{s}}, \qquad \frac{dz}{ds} = \frac{dz}{d\bar{s}} \frac{1}{\lambda} = \frac{d\bar{z}}{d\bar{s}}.$$

Substituting the "bar" variables into (3.5) and setting $w = w_d \rho$, we see

$$\lambda \bar{r} \bar{\sigma}_m (\lambda^2 b_d) \frac{1}{\lambda} \frac{d\theta}{d\bar{s}} = -\lambda \bar{r} w_d \rho \sin\theta - b\lambda \bar{r}(\lambda \bar{z} + \lambda \bar{a}). \tag{3.24}$$

Dividing (3.24) by $\lambda^2 b_d$, and substituting the definition of $k\,\Sigma$, we obtain

$$\bar{r} \bar{\sigma}_m \frac{d\theta}{d\bar{s}} = -k\,\Sigma \rho \bar{r} \sin\theta - \tau_b \bar{r}(\bar{z} + \bar{a}), \tag{3.25}$$

where $\tau_b = b/b_d$. In general, $\tau_b \geq 1$, with $\tau_b = 1$ at float. Since b is known as a function of altitude and b_d is specified at the design stage, τ_b is also known as a function of altitude.

In a similar way, from (3.6) with $\sigma_c = 0$ and $w = w_d \rho$, we find

$$\frac{1}{\lambda} \frac{d}{d\bar{s}} (b_d \lambda^3 \bar{r} \bar{\sigma}_m) = \lambda w_d \rho \bar{r} \cos\theta. \tag{3.26}$$

Dividing through by $\lambda^2 b_d$ and substituting the definition of $k\,\Sigma$, we obtain

$$\frac{d}{d\bar{s}} (\bar{r} \bar{\sigma}_m) = k\,\Sigma \bar{r} \rho \cos\theta. \tag{3.27}$$

Downloaded 03/31/14 to 128.210.126.199. Redistribution subject to SIAM license or copyright; see http://www.siam.org/journals/ojsa.php

For completeness, we note that

$$\frac{d\bar{r}}{d\bar{s}} = \sin\theta, \qquad \frac{d\bar{z}}{d\bar{s}} = \cos\theta.$$

If we define $\bar{A} = A/\lambda^2$ and $\bar{V} = V/\lambda^3$, we find that

$$\frac{d\bar{A}}{d\bar{s}} = 2\pi\bar{r}, \qquad \frac{d\bar{V}}{d\bar{s}} = \pi\bar{r}^2\frac{d\bar{z}}{d\bar{s}} = \pi\bar{r}^2\cos\theta. \tag{3.28}$$

Based on physical principles, the tension is strictly increasing as a function of $\bar{s}$, i.e., $(\bar{r}\bar{\sigma}_m)'(\bar{s}) > 0$. For this reason, we can define $\bar{m} = (\bar{r}\bar{\sigma}_m)^{-1}$. Substituting $\bar{m}$ into (3.25) and (3.27) and using

$$\frac{d}{d\bar{s}}(\bar{r}\bar{\sigma}_m) = -\frac{1}{\bar{m}^2}\frac{d\bar{m}}{d\bar{s}},$$

we obtain the model equations for a natural-shape balloon,

$$\frac{d\theta}{d\bar{s}} = -\bar{m}(k\,\Sigma\rho\bar{r}\sin\theta + \tau_b\bar{r}(\bar{z}+\bar{a})), \tag{3.29}$$

$$\frac{d\bar{m}}{d\bar{s}} = -k\Sigma\rho\bar{r}\bar{m}^2\cos\theta, \tag{3.30}$$

$$\frac{d\bar{r}}{d\bar{s}} = \sin\theta, \tag{3.31}$$

$$\frac{d\bar{z}}{d\bar{s}} = \cos\theta. \tag{3.32}$$

The form of the Σ-shape equations presented in [1], [8], and [9] involves $\bar{r}\bar{\sigma}_m$ as the unknown instead of $\bar{m}$. The two formulations are equivalent, but we found it was easier to establish existence results using (3.29)–(3.32).

When computing an ascent shape (assuming the generating curve $(\bar{Z}_d(s), \bar{R}_d(s))$, $0 \le \bar{s} \le \bar{\ell}_d$ is known), we set $\rho(\bar{s}) = \bar{R}_d(\bar{s})/\bar{r}(\bar{s})$. Equations (3.29)–(3.30) simplify to

$$\frac{d\theta}{d\bar{s}} = -\bar{m}(k\,\Sigma\bar{R}_d\sin\theta + \tau_b\bar{r}(\bar{z}+\bar{a})), \tag{3.33}$$

$$\frac{d\bar{m}}{d\bar{s}} = -k\Sigma\bar{R}_d\bar{m}^2\cos\theta. \tag{3.34}$$

Note that even though $\bar{r} = 0$ at the top and bottom of the balloon, the definition of ρ does not lead to singularities in (3.33)–(3.34).

The boundary conditions at $\bar{s} = 0$ are given in terms of the unknown parameter θ_0 as follows:

$$\theta(0) = \theta_0, \tag{3.35}$$

$$\bar{m}(0) = 2\pi\cos\theta_0, \tag{3.36}$$

$$\bar{r}(0) = 0, \tag{3.37}$$

$$\bar{z}(0) = 0, \tag{3.38}$$

where in (3.36), we have used the fact that $L/(\lambda^3 b_d) = 1$. Equations (3.35)–(3.38) are supplemented by two side conditions at the top of the balloon,

$$|\theta(\bar{\ell};\tau_b,\theta_0,\bar{\ell},\bar{a})| - \tfrac{1}{2}\pi = 0, \tag{3.39}$$

$$\bar{r}(\bar{\ell};\tau_b,\theta_0,\bar{\ell},\bar{a}) = 0, \tag{3.40}$$

Downloaded 03/31/14 to 128.210.126.199. Redistribution subject to SIAM license or copyright; see http://www.siam.org/journals/ojsa.php

where $\bar{\ell}$ is the (unknown) gore length.

Remark. We have modified (3.39) so that we can consider multicell shapes (see section 4.1) with an even or odd number of cells. If the number of cells is even, then $\theta(\bar{\ell}) = +\pi/2$. If the number of cells is odd, then $\theta(\bar{\ell}) = -\pi/2$.

At float, $\tau_b = 1, \bar{a} = 0, \rho = 1$, and the parameters L, b_d, w_d are known. Equations (3.39)–(3.40) reduce to

$$|\theta(\bar{\ell}; 1, \theta_0, \bar{\ell}, 0)| - \tfrac{1}{2}\pi = 0, \tag{3.41}$$

$$\bar{r}(\bar{\ell}; 1, \theta_0, \bar{\ell}, 0) = 0. \tag{3.42}$$

A solution of (3.29)–(3.32), (3.35)–(3.38), and (3.41)–(3.42) defines the float shape. The solution of (3.41)–(3.42) is denoted by $(\theta_0, \bar{\ell}) = (\theta_{0,d}, \bar{\ell}_d)$. The generating curve in this case is denoted by $(\bar{z}, \bar{r}) = (\bar{Z}_d(\bar{s}), \bar{R}_d(\bar{s}))$, where $0 \le \bar{s} \le \bar{\ell}_d$.

When computing an axisymmetric ascent shape, $(\bar{Z}_d(\bar{s}), \bar{R}_d(\bar{s}))$ and $\bar{\ell}_d$ are known from the design stage, $\rho = \bar{R}_d/\bar{r}$, and τ_b is determined by the altitude. In this case, (3.39)–(3.40) reduce to

$$|\theta(\bar{\ell}_d; \tau_b, \theta_0, \bar{\ell}_d, \bar{a})| - \tfrac{1}{2}\pi = 0, \tag{3.43}$$

$$\bar{r}(\bar{\ell}_d; \tau_b, \theta_0, \bar{\ell}_d, \bar{a}) = 0. \tag{3.44}$$

The axisymmetric model ascent shape is given by the solution of (3.29)–(3.32), (3.35)–(3.38), and (3.43)–(3.44). The solution of (3.43)–(3.44) is denoted by $(\theta_0, \bar{a}) = (\theta_0^*, \bar{a}^*)$.

For convenience, we introduce two parameter sets

$$\mathcal{P}_d = \left\{(\tau_b, \theta_0, \bar{\ell}, \bar{a}) \mid \tau_b = 1,\ 0 < \theta_0 < \tfrac{1}{2}\pi,\ 0 < \bar{\ell} < \ell_{\max},\ \bar{a} = 0\right\}, \tag{3.45}$$

$$\mathcal{P}_a = \left\{(\tau_b, \theta_0, \bar{\ell}, \bar{a}) \mid\ 1 \le \tau_b,\ 0 < \theta_0 < \tfrac{1}{2}\pi,\ \bar{\ell} = \bar{\ell}_d,\ -\bar{a}_{\max} < \bar{a} \le 0\right\} \tag{3.46}$$

for some positive numbers $a_{\max}$ and $\ell_{\max}$, where $\bar{a}$ corresponds to a position along the center axis of the balloon where the differential pressure changes sign. For a balloon in quasi-steady state equilibrium, we can choose $\bar{a}_{\max} = \ell_{\max}$. Setting $\mathbf{p} = (\tau_b, \theta_0, \bar{\ell}, \bar{a})$,

$$\mathbf{u} = \begin{pmatrix} u_1(\bar{s}; \mathbf{p}) \\ u_2(\bar{s}; \mathbf{p}) \\ u_3(\bar{s}; \mathbf{p}) \\ u_4(\bar{s}; \mathbf{p}) \end{pmatrix} = \begin{pmatrix} \theta(\bar{s}; \tau_b, \theta_0, \bar{\ell}, \bar{a}) \\ \bar{m}(\bar{s}; \tau_b, \theta_0, \bar{\ell}, \bar{a}) \\ \bar{r}(\bar{s}; \tau_b, \theta_0, \bar{\ell}, \bar{a}) \\ \bar{z}(\bar{s}; \tau_b, \theta_0, \bar{\ell}, \bar{a}) \end{pmatrix}, \qquad \mathbf{v}_1 = \begin{pmatrix} \theta_0 \\ 2\pi\cos\theta_0 \\ 0 \\ 0 \end{pmatrix}, \tag{3.47}$$

we find that (3.29)–(3.32) and (3.35)–(3.40) can be written in the form

$$\dot{\mathbf{u}} = \mathbf{h}(\mathbf{u}; \mathbf{p}), \tag{3.48}$$

$$\mathbf{u}(0) = \mathbf{v}_1, \tag{3.49}$$

$$\mathbf{g}(\mathbf{v}_1, \mathbf{u}(\bar{\ell}, \mathbf{u}(\bar{\ell})); \mathbf{p}) = \mathbf{0}, \tag{3.50}$$

where $\mathbf{g}$ represents equations (3.39)–(3.40), $\mathbf{h}$ represents the right-hand side of (3.29)–(3.32), and " $\dot{}$ " represents differentiation with respect to $\bar{s}$. When computing an ascent shape, both $\mathbf{h}$ and $\mathbf{g}$ will depend implicitly on $\bar{R}_d$.

The existence of a solution of (3.48)–(3.50) follows from the standard theory for nonlinear boundary value problems. Defining

$$\mathcal{R}_\gamma = \{(\bar{s}, \mathbf{u}) \mid 0 \le \bar{s} \le \ell_{\max}, ||\mathbf{u}|| < \gamma\},$$

where $||\mathbf{u}|| = \max_{1 \le i \le 4} |u_i|$, it is easy to verify that $\partial\mathbf{h}/\partial\mathbf{u}$ is continuous on $\mathcal{R}_\gamma$ for any $\mathbf{p} \in \mathcal{P}_d$ or $\mathbf{p} \in \mathcal{P}_a$. By [6, p. 6, Theorem 1.1.4], (3.48)–(3.50) has a solution for any such $\mathbf{p}$. The components of $\mathbf{p}$ are chosen so that (3.50) is satisfied.

Downloaded 03/31/14 to 128.210.126.199. Redistribution subject to SIAM license or copyright; see http://www.siam.org/journals/ojsa.php

TABLE 4.1
Single-, double-, and triple-cell float shapes with $w = 0$.

k	$\theta_{0,d}^k$ (deg)	$\bar{\ell}_d^k$	$(\bar{r}_{\max}, \bar{z})$	$\bar{z}_{\max}$	$\bar{\mathcal{A}}_d$
1	50.15000	1.994494	(0.6522, 0.8469)	1.28419	4.91652
2	43.8817	3.127983	(0.5386,0.8235)	2.025492	6.118503
3	40.6947	4.067583	(0.4875,0.8466)	2.637060	6.951056

TABLE 4.2
Natural-shape balloons with $\Sigma = 0.4$, $\bar{\ell} = 2.870569$, and $L = 1$.

τ_b	θ_0	$\hat{s}_0$	$(\bar{r}(\hat{s}_0), \bar{z}(\hat{s}_0))$	$\bar{a}$	$(\bar{r}_{\max}, z)$	$\bar{z}_{\max}$	J	CPU (min)
1.00	67.90600	0.00082	(0.001, 0.000)	−0.001	(1.036, 0.954)	1.5914	1	-
1.10	50.91575	0.26119	(0.206, 0.161)	−0.470	(0.982, 1.133)	1.7618	5	6.328
1.20	40.60027	0.32262	(0.228, 0.228)	−0.650	(0.943, 1.233)	1.8550	5	4.421
1.30	33.21361	0.34750	(0.225, 0.264)	−0.764	(0.911, 1.309)	1.9194	5	3.486
1.40	27.60188	0.37203	(0.224, 0.295)	−0.847	(0.884, 1.374)	1.9680	5	3.488
1.50	23.18158	0.38444	(0.217, 0.314)	−0.912	(0.860, 1.431)	2.0069	5	3.464
2.50	5.26965	0.48621	(0.183, 0.439)	−1.254	(0.708, 1.737)	2.2000	5	4.395
6.00	0.09789	0.60325	(0.128, 0.575)	−1.654	(0.519, 2.049)	2.3955	5	5.430
15.00	0.00007	0.69838	(0.089, 0.681)	−1.965	(0.379, 2.267)	2.5296	5	6.603
40.00	0.00000	0.77726	(0.061, 0.766)	−2.213	(0.272, 2.435)	2.6279	5	9.821
100.00	0.00000	0.83811	(0.046, 0.830)	−2.384	(0.200, 2.555)	2.6928	10	19.503
200.00	0.00000	0.87224	(0.037, 0.865)	−2.484	(0.158, 2.621)	2.7299	20	36.178
300.00	0.00000	0.88787	(0.032, 0.882)	−2.532	(0.138, 2.652)	2.7478	20	36.591
400.00	0.00000	0.89785	(0.029, 0.893)	−2.563	(0.126, 2.671)	2.7591	40	92.715
500.00	0.00000	0.90566	(0.027, 0.901)	−2.585	(0.117, 2.687)	2.7671	40	91.028
600.00	0.00000	0.91035	(0.025, 0.906)	−2.602	(0.110, 2.697)	2.7732	40	91.448
700.00	0.00000	0.91533	(0.024, 0.911)	−2.615	(0.104, 2.705)	2.7781	80	335.223
800.00	0.00000	0.91924	(0.023, 0.915)	−2.626	(0.100, 2.712)	2.7822	80	331.680
900.00	0.00000	0.92236	(0.022, 0.918)	−2.636	(0.096, 2.720)	2.7856	80	329.954
1000.00	0.00000	0.92466	(0.021, 0.921)	−2.644	(0.092, 2.725)	2.7886	80	254.220

4. Numerical solutions. An ordinary shooting method will be used to compute float shapes. For our examples, we choose $b_d = 10^{-3}$ lbs/ft^3 and $L = 1$ lb, so $\lambda = 10$. In section 4.1, we present our results on float shapes with zero film weight. To illustrate the fact that solutions need not be unique, we include several multicell solutions for the design shape. The results on balloons with zero film weight are summarized in Table 4.1. Increasing the film weight per unit area leads to a float shape that is more oblate. In section 4.2, we consider balloon shapes based on $w_d = 0.00217$ lbs/ft^2. This choice leads to a value of $\Sigma = 0.4$ and corresponds to a typical value used in large scientific balloons. In this case, we also include the corresponding family of ascent shapes. These results are summarized in Table 4.2.

4.1. Ordinary shooting method. A shooting method was implemented to determine the design shapes using Matlab and its utilities fsolve and ode45. Solutions of (3.50) were computed using fsolve. To determine the values of $\theta(\bar{\ell})$ and $\bar{r}(\bar{\ell})$ for fsolve, (3.48) were integrated from $0 \le \bar{s} \le \bar{\ell}$ using ode45 with the initial conditions (3.49). We began with an initial guess for θ_0 and $\bar{\ell}$. We found the solution process to be robust and we were able to converge to a solution even if a poor initial guess was used. A solution of (3.48)–(3.50) with $(\theta_0, \bar{\ell}) = (\theta_{0,d}, \bar{\ell}_d)$ was accepted once the residuals in (3.50) were sufficiently small (i.e., on the order of 10^{-3}). Data on the float shape for a balloon film with weight $w = 0$ is presented in Table 4.1. We define $\bar{r}_{\max} = \max_{0 \le \bar{s} \le \bar{\ell}_d} |\bar{r}(\bar{s})|$ and $\bar{z}_{\max} = \max_{0 \le \bar{s} \le \bar{\ell}_d} |\bar{z}(\bar{s})|$. The generating curves for these shapes are presented in Figure 4.1.

While the solutions of (3.48)–(3.49) are unique for a fixed $\mathbf{p}$, in general, solutions

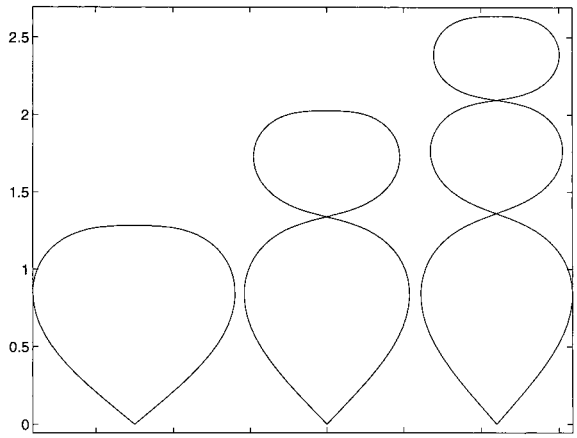

FIG. 4.1. *Design shapes with k cells, $k = 1, 2, 3$, $w = 0$, and $\mathcal{V}_d = 1$.*

of the boundary value problem (3.48)–(3.49) need not be unique. For $\bar{\ell}_{\max}$ sufficiently large, there exist more than one solution of (3.48)–(3.49) (but with different values of ℓ_d). This was first suggested by the "double-cell" shape presented in [1, Vol. I, pp. 3–14], where $\theta(\bar{\ell}) = +\frac{1}{2}\pi$. A triple-cell configuration with $\theta(\bar{\ell}) = -\frac{1}{2}\pi$ was found (see Figure 4.1). Numerical evidence suggests that a configuration with k cells is possible for any k if $\bar{\ell}$ is chosen appropriately. We can index these solutions by $(\theta^k_{0,d}, \bar{\ell}^k_d)$, where k is the number of cells in the corresponding shape. Since the governing equations depend continuously on the parameters, we can draw the same conclusions about a balloon with nonzero film weight. From a practical standpoint, the multicell configurations are usually disregarded, because they require more balloon material to lift a given payload to float than a balloon with a single cell. There are also problems in handling and launching a balloon with more than one cell.

The data presented in Table 4.1 for the single-cell shape agrees with the data in [10, Table X]. Data presented on the double-cell shape is in agreement with [1, Vol. I, pp. 3–14].

4.2. Parallel shooting method. The ordinary shooting method is not very effective in solving (3.48)–(3.49) when $\tau_b \geq 10$. In this range, θ_0 is close to zero and it is very difficult to satisfy the side conditions at $\bar{s} = \bar{\ell}_d$. A parallel shooting method avoids this difficulty in a very natural way. In this section, we outline a parallel shooting method to solve the Σ-shape equations. Following the notation introduced in [7], we break the interval $[0, \bar{\ell}_d]$ into J subintervals,

$$[\bar{s}_0, \bar{s}_1],\ [\bar{s}_1, \bar{s}_2],\ \ldots,\ [\bar{s}_{J-1}, \bar{s}_J],$$

and then enforce a continuity condition at each interior endpoint in addition to the side conditions (3.50). In particular, we consider,

$$\dot{\mathbf{u}}_j = \mathbf{h}(\bar{s}, \mathbf{u}_j), \quad \bar{s}_{j-1} \leq \bar{s} \leq \bar{s}_j, \tag{4.1}$$

$$\mathbf{u}_j(\bar{s}_{j-1}) = \mathbf{v}_j, \quad 1 \leq j \leq J, \tag{4.2}$$

Downloaded 03/31/14 to 128.210.126.199. Redistribution subject to SIAM license or copyright; see http://www.siam.org/journals/ojsa.php

Downloaded 03/31/14 to 128.210.126.199. Redistribution subject to SIAM license or copyright; see http://www.siam.org/journals/ojsa.php

along with the equations,

$$\begin{bmatrix} \mathbf{g}(\mathbf{v}_1, \mathbf{u}_J(\bar{\ell}, \mathbf{v}_J)) \\ \mathbf{v}_2 - \mathbf{u}_1(\bar{s}_1, \mathbf{v}_1) \\ \mathbf{v}_3 - \mathbf{u}_2(\bar{s}_2, \mathbf{v}_2) \\ \vdots \\ \mathbf{v}_J - \mathbf{u}_{J-1}(\bar{s}_{J-1}, \mathbf{v}_{J-1}) \end{bmatrix} = \mathbf{0}. \tag{4.3}$$

A new independent variable $\hat{s}$ is introduced,

$$\hat{s} = \frac{\bar{s} - s_{j-1}}{\triangle_j}, \quad \triangle_j = \bar{s}_j - \bar{s}_{j-1}, \quad j = 1, \ldots, J,$$

so that $0 \le \hat{s} \le 1$. Setting $\hat{\mathbf{u}}_j(\hat{s}) = \mathbf{u}(\bar{s}_{j-1} + \hat{s}\triangle_j)$,

$$\hat{\mathbf{h}}_j(\hat{s}, \mathbf{u}_j(\hat{s})) = \triangle_j \mathbf{h}(\bar{s}_{j-1} + \hat{s}\triangle_j, \mathbf{u}_j(\hat{s})),$$

we see that (4.1)–(4.3) can be rewritten as

$$\hat{\mathbf{u}}' = \hat{\mathbf{h}}(\hat{s}, \hat{\mathbf{u}}), \ 0 \le \hat{s} \le 1, \tag{4.4}$$

$$\hat{\mathbf{u}}(0) = \hat{\mathbf{v}}, \tag{4.5}$$

$$\hat{\mathbf{g}}(\hat{\mathbf{u}}(0), \hat{\mathbf{u}}(1)) = \begin{bmatrix} \hat{\mathbf{g}}(\hat{\mathbf{u}}_1(0), \hat{\mathbf{u}}_J(1)) \\ \hat{\mathbf{u}}_2(0) - \hat{\mathbf{u}}_1(1) \\ \vdots \\ \hat{\mathbf{u}}_J(0) - \hat{\mathbf{u}}_{J-1}(1) \end{bmatrix} = \mathbf{0}, \tag{4.6}$$

respectively. Differentiation with respect to $\hat{s}$ is denoted by "$'$" and

$$\hat{\mathbf{u}} = \begin{bmatrix} \hat{\mathbf{u}}_1 \\ \hat{\mathbf{u}}_2 \\ \vdots \\ \hat{\mathbf{u}}_J \end{bmatrix}, \quad \hat{\mathbf{h}} = \begin{bmatrix} \hat{\mathbf{h}}_1 \\ \hat{\mathbf{h}}_2 \\ \vdots \\ \hat{\mathbf{h}}_J \end{bmatrix}, \quad \hat{\mathbf{v}} = \begin{bmatrix} \mathbf{v}_1 \\ \mathbf{v}_2 \\ \vdots \\ \mathbf{v}_J \end{bmatrix}. \tag{4.7}$$

When $1 < \tau_b < 40$, we set $J = 5$. For much smaller volumes, we increased J accordingly (see Table 4.2).

In Table 4.2, we present data on natural-shape balloons with $w_d = 0.00217$, a film weight that leads to $\Sigma = 0.4$. The case $\tau_b = 1$ was computed using an ordinary shooting method. The position along the gore corresponding to the zero differential pressure level is denoted by $\hat{s}_0$. The corresponding solutions are presented in Figure 4.2. Our results in Table 4.2 are in good agreement with the data presented in [10, Table 3] (the last three columns of [10, Table 3] need to be rescaled by a factor of 2.87047 before comparing with the appropriate results in Table 4.2). For large values of τ_b, the results in Table 4.2 and [10, Table 3] differ slightly, because we did not use Smalley's ad hoc method of a rope section in our computations.

5. Concluding remarks. The existence of solutions to the model equations for natural-shape balloons follows from the standard theory for systems of ordinary differential equations (see [7]). Numerically, the model float shapes can be determined by applying a standard shooting method. The model ascent shapes are difficult to compute for volumes less than 10% of $\mathcal{V}_d$, because the differential equations are extremely

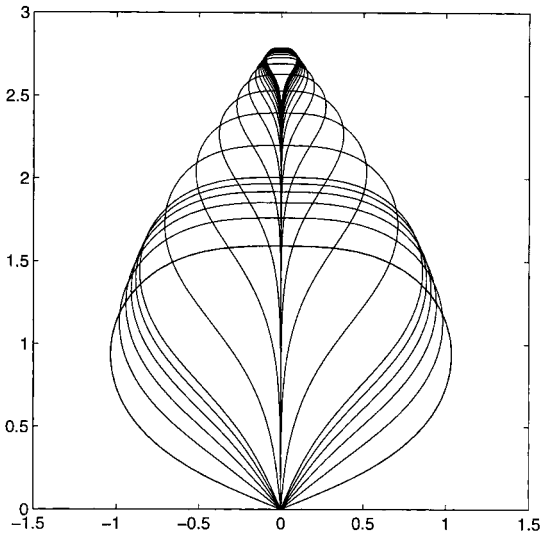

FIG. 4.2. *Natural-shape balloons,* $\Sigma = 0.4$.

sensitive to the choice of parameter values for the boundary and side conditions. The difficulty is related to the fact that the gas bubble is concentrated near the top of the balloon configuration and the angle $\theta(\bar{s})$ is very small for a significant portion of the interval $[0, \bar{\ell}_d]$. The parallel shooting method of Keller (see [6] and [7]) works very well in avoiding this difficulty, without the need of the ad hoc assumption of a rope section. We are able to compute ascent shapes with a volume as small as 0.01% of $\mathcal{V}_d$ using a parallel shooting method. Our results are in agreement with previous work (see [1] and [10]).

REFERENCES

[1] ANON., *Research Development in the Field of High Altitude Plastic Balloons*, NONR–710(01a) Reports, Department of Physics, University of Minnesota, Minneapolis, MN, 1951–1956.
[2] S. S. ANTMAN, *Nonlinear Problems of Elasticity*, Springer-Verlag, New York, 1995.
[3] F. BAGINSKI, *Mathematical Modeling of Energy Minimizing Off-Design Shapes of Large Scientific Balloons I*, Final Report for NAG5-697, NASA Balloon Projects, Wallops Flight Facility, Wallops Island, VA, Jan. 1994.
[4] F. BAGINSKI, *Modeling nonaxisymmetric off-design shapes of large scientific balloons*, AIAA J., 34 (1996), pp. 400–407.
[5] F. BAGINSKI AND S. RAMAMURTI, *Variational principles for the ascent shapes of large scientific balloons*, AIAA J., 33 (1995), pp. 764–768.
[6] H. B. KELLER, *Numerical Methods for Two-Point Boundary-Value Problems*, Blaisdell, Waltham, MA, 1968.
[7] H. B. KELLER, *Numerical Two-Point Boundary-Value Problems*, Dover, New York, 1982.
[8] A. L. MORRIS, ED., *Scientific Ballooning Handbook*, NCAR-TN-99, National Center for Atmospheric Research, Boulder, CO, May 1975.
[9] J. H. SMALLEY, *Determination of the Shape of a Free Balloon*, Scientific Report No. 2, AFRL 64-734, Air Force Cambridge Research Laboratories, Bedford, MA, Dec. 1963.
[10] J. H. SMALLEY, *Balloon Shapes and Stresses below the Design Altitude*, NCAR-TN-25, National Center for Atmospheric Research, Boulder, CO, Dec. 1996.

Downloaded 03/31/14 to 128.210.126.199. Redistribution subject to SIAM license or copyright; see http://www.siam.org/journals/ojsa.php